

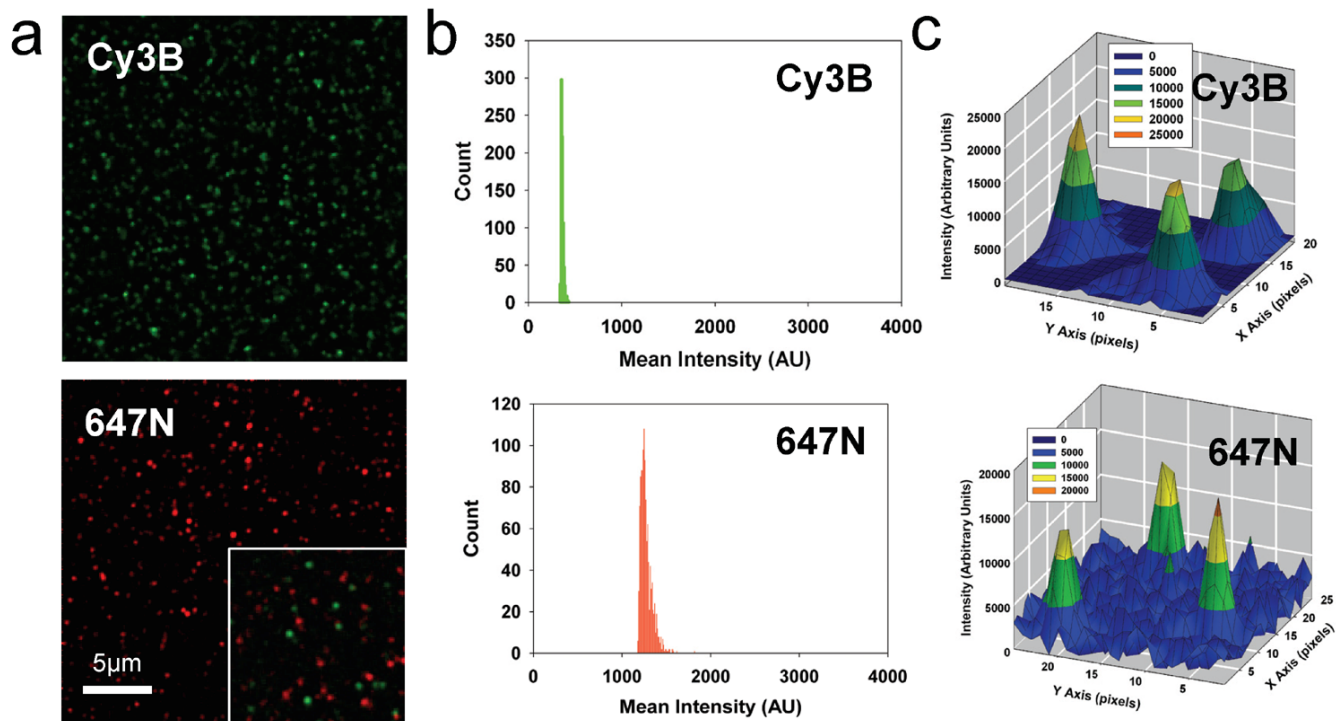
Single molecule–sensitive probes for imaging RNA in live cells

Philip J Santangelo, Aaron W Lifland, Paul Curt, Yukio Sasaki, Gary J Bassell, Michael E Lindquist & James E Crowe Jr

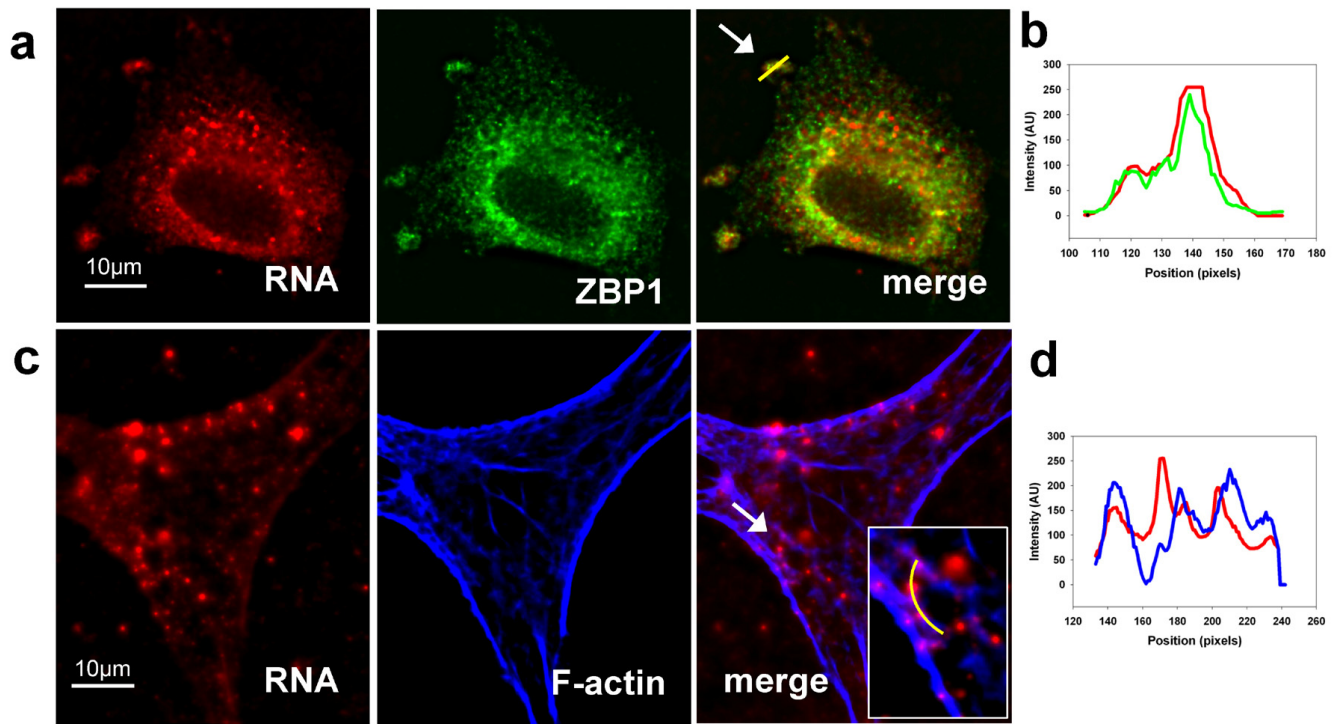
Supplementary figures and text:

Supplementary Figure 1	Images of single MTRIPs on glass surface.
Supplementary Figure 2	MTRIP targeting of native β -actin mRNA in motile cells.
Supplementary Figure 3	Quantification of 3D colocalization of β -actin mRNA and ZBP1 in a motile epithelial cell.
Supplementary Figure 4	Simultaneous targeting of arp2 and β -actin mRNA in primary chicken embryonic fibroblasts using MTRIP probes.
Supplementary Figure 5	Validation of hRSV targeted MTRIPs in infected and non-infected cells and via RNA-protein colocalization.
Supplementary Figure 6	Quantification of 3D colocalization of RSV genomic RNA and the nucleocapsid protein in an infected epithelial cell.
Supplementary Figure 7	Comparison of RSV granule detection using tetravalent MTRIPs and monovalent probes.
Supplementary Figure 8	Time-lapse imaging of granule fusion.
Supplementary Figure 9	Time-lapse imaging of granule splitting.
Supplementary Figure 10	Effects of SLO on A549 cells via live-dead assay.
Supplementary Table 1	Ligands for MTRIPs utilized within this paper.
Supplementary Results	

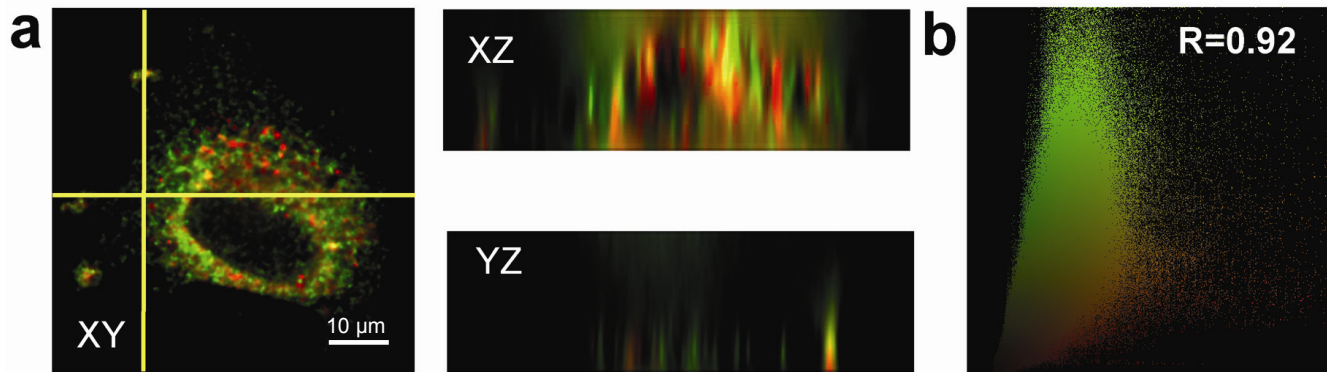
Note: Supplementary Videos 1–8 are available on the Nature Methods website.



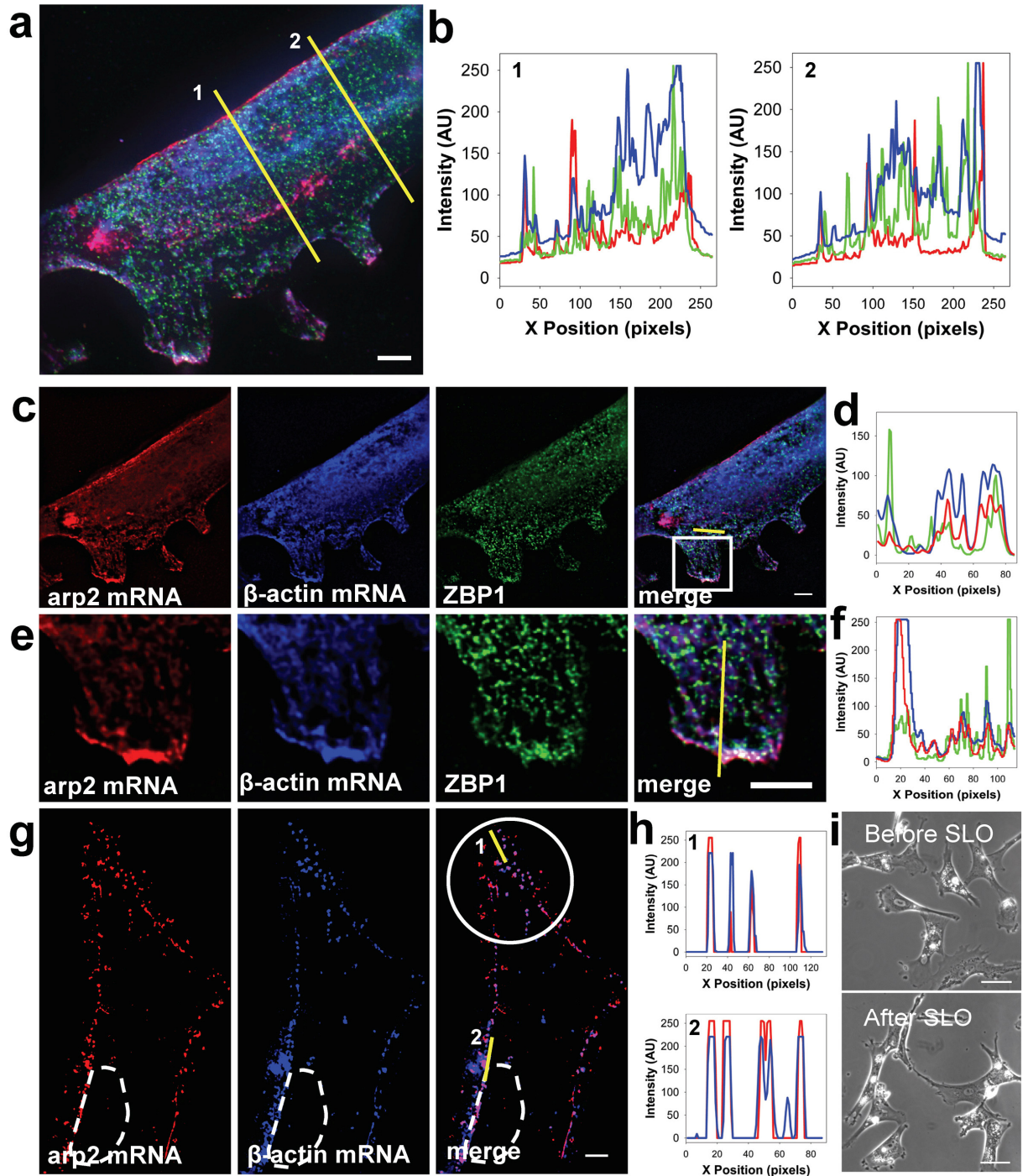
Supplementary Figure 1. Images of single MTRIPs on glass surface. (a) Images of single Cy3B and Atto 647N probes, respectively, at 2 nM. (Inset depicts image of a mixture of Cy3B and Atto 647N MTRIPs demonstrating probe independence.) (b) Histograms of the mean intensity within each diffraction-limited spot constructed from 750-1000 detected probes. The unimodal histograms and (c) three-dimensional intensity profiles of representative probes post-deconvolution, additionally demonstrate that single probes were imaged.



Supplementary Figure 2. Single MTRIP targeting of native β -actin mRNA in motile A549 cells showing specific targeting when RNA aggregates spatially. (a,b) MTRIPs using human β -actin probe 1 (red), delivered at 30 nM, colocalize (yellow) with ZBP1 (green), especially in the ends of pseudopods. Colocalization is observed both in the merge image, as well as in the intensity profile drawn through one of the pseudopods. (c,d) β -actin mRNA are also known to colocalize with F-actin, and MTRIPs (red) delivered at 1 nM show colocalization (purple) with phalloidin-stained stress fibers (blue). Inset image within merge focuses on a region of significant colocalization, and intensity profile shows correlation of F-actin signal (blue) with MTRIPs (red). β -actin mRNA images were taken using epifluorescence microscopy, deconvolved, and a single optical plane is shown.

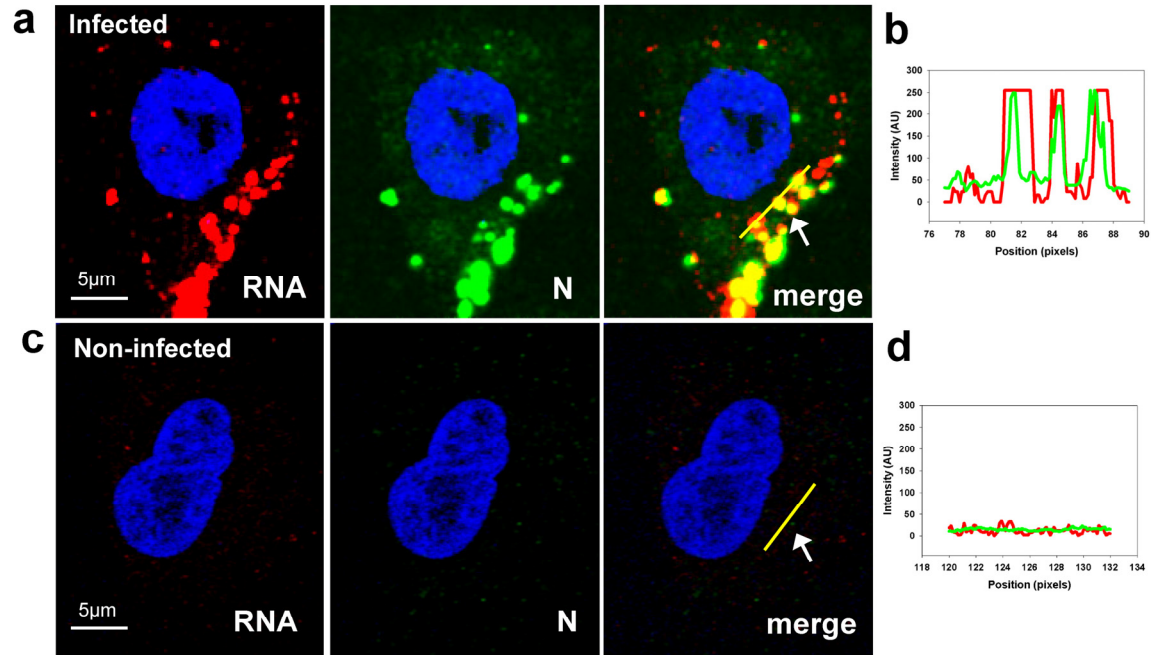


Supplementary Figure 3. Quantification of 3D colocalization of single (human β -actin mRNA probe 1) MTRIP targeted to β -actin mRNA and ZBP1 in a motile epithelial cell. (a) XY, XZ, and YZ profiles at location designated by the yellow cross-hair are provided as evidence of colocalization within both a pseudopod (YZ) and within the perinuclear region (XZ). Strong yellow signal can be observed in both cross-sections. (b) From the 3D reconstruction of voxels, a scatter plot of voxel intensities was generated and the Manders overlap coefficient calculated. In this case the Manders overlap coefficient was 0.92, suggesting significant colocalization in three dimensions.

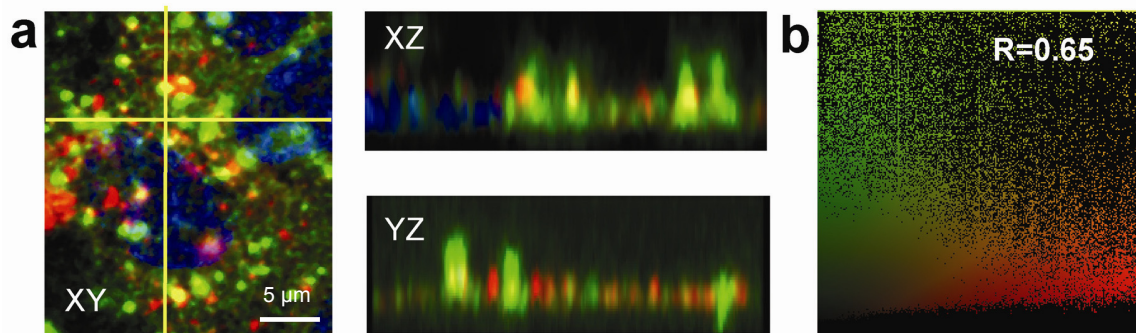


Supplementary Figure 4

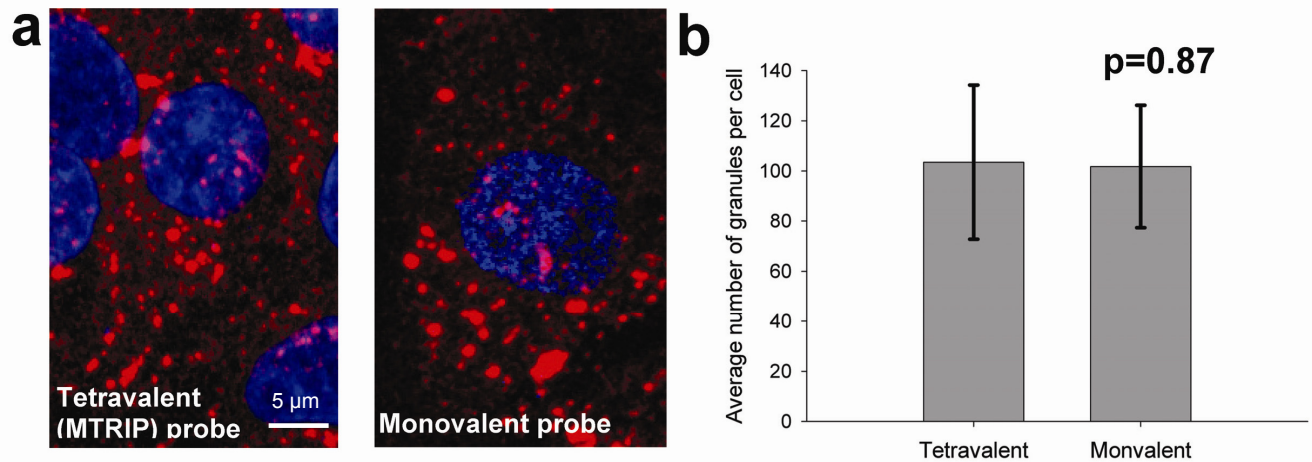
Supplementary Figure 4. Imaging of arp2 and β -actin mRNA and ZBP1 in primary chicken embryonic fibroblasts (CEF). (a) Extended view of arp2 (red) and β -actin (blue) mRNA, and ZBP1 (green) in a motile primary CEF. Arp2 and β -actin mRNA were tagged with 3 MTRIPs (all probes in Supplementary Table) each labeled with Cy3B and Atto-647N via live-cell hybridization via SLO delivery, post-fixed in paraformaldehyde and immunostained with a guinea pig anti-ZBP1 antibody. (b) Intensity profiles through two cross-sections (denoted 1 and 2) of the extended view reveal two types of localization; within the perinuclear region, β -actin mRNA signal is not correlated with the arp2 mRNA signal, especially from approximately pixel 100 to 225 in profile 1 and from 100 to 150 and 175 to 225 in profile 2; ZBP1 and β -actin mRNA are correlated within these same regions. (c, d, e, f) While, from a single plane image of the cell, near the glass surface and within a lamellipodium (indicated by the white box), colocalization of arp2 (red) mRNA, β -actin (blue) mRNA, and ZBP1 (green) can be observed especially within the lamellipodium near the leading edge. (g,h) Live cell image of arp2 (red) and β -actin (blue) mRNA tagged with the same MTRIPs as above; granules within a protrusion of CEF show significant colocalization. Dashed white region represents the cell nucleus. (i) Phase contrast images of primary CEFs before and after SLO exposure show no significant changes in cellular morphology. The images were taken 20 minutes after SLO exposure. The white bars in (a,c,g,e) represent 5 μ m and in (i) represent 50 μ m.



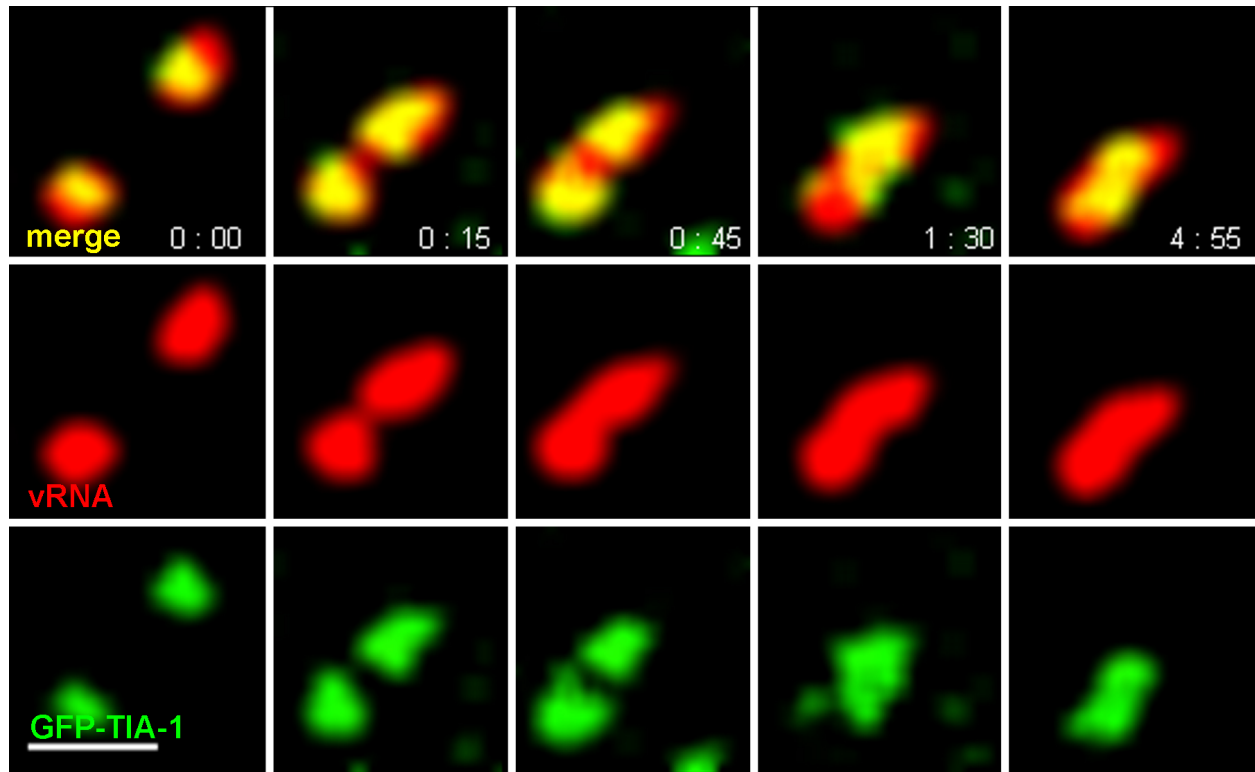
Supplementary Figure 5. Validation of hRSV-targeted MTRIP specificity. (a,b) MTRIPs targeted the viral genomic RNA of hRSV (red) and colocalized (yellow) with hRSV nucleocapsid protein (green) in infected cells. DAPI staining (blue) stains the nucleus of the cell. (c,d) Little background was observed in non-infected cells. Colocalization was observed in the images, and quantified in intensity profiles along the yellow line, denoted by the white arrow.



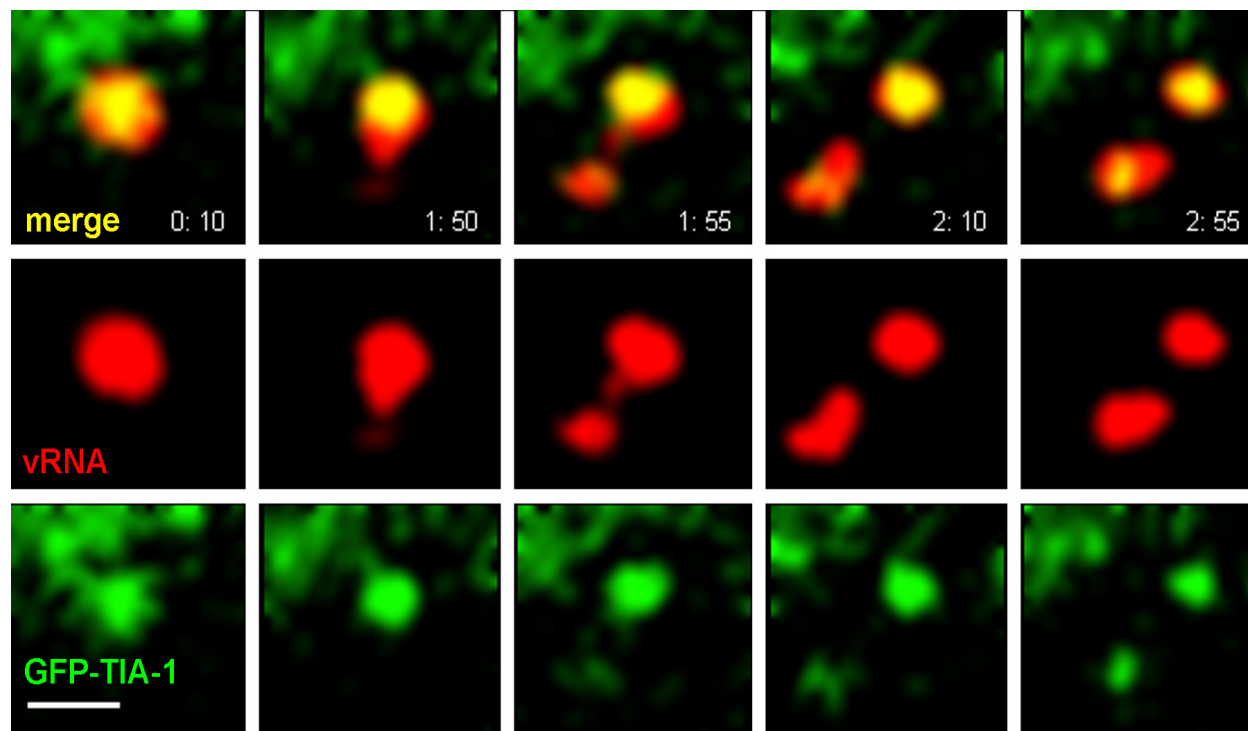
Supplementary Figure 6. Quantification of 3D colocalization of MTRIP targeted to hRSV genomic RNA (red) and nucleocapsid protein (green) in an epithelial cell. (a) XY, XZ, and YZ profiles at location designated by the yellow cross-hair are provided as evidence of colocalization. Strong yellow signal representing colocalization can be observed in both cross-sections. (b) From the 3D reconstruction of voxels, a scatter plot of voxel intensities was generated, and the Manders overlap coefficient calculated. In this case the Manders overlap coefficient was 0.65, demonstrating colocalization in three dimensions.



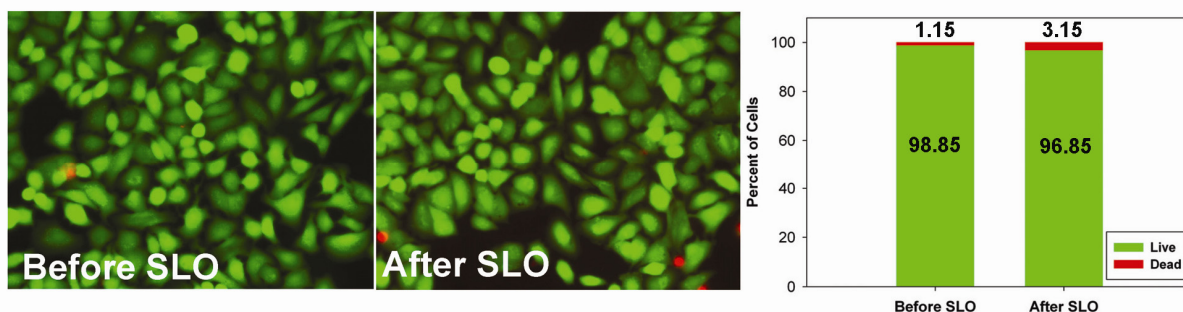
Supplementary Figure 7. Comparison of tetraivalent MTRIPs and monovalent probes (single multiply-labeled ligand) both targeted to hRSV genomic RNA (red). (a) Representative images from infections targeted by each probe type. Both sets of cells were plated simultaneously and infected from the same lot of virus. It should be noted that even though the number of granules detected is statistically similar, the photomultiplier voltage settings on the laser scanning confocal was approximately 4 times higher for the monovalent probe, which was expected. By combining 4 ligands, the resulting MTRIPs were 4 times brighter, a necessity for the live-cell imaging in Fig. 2 and 3. The nucleus (blue) was stained with DAPI. (b) RNA granules from over 30 cells for both the tetraivalent and monovalent probes were counted via Volocity using the same conditions; statistical similarity of the distributions was determined with the Wilcoxon-Mann-Whitney test, resulting in a p value of 0.87, which strongly suggests that the samples originated from the same population. This provides strong evidence that MTRIPs do not significantly aggregate RNA; RNA aggregation would have resulted in the detection of different numbers of RNA granules.



Supplementary Figure 8: Time-lapse imaging of granule fusion. Time-lapse imaging reveals, over a 5 minute period, the fusion of a viral RNA granule that is well associated with GFP-TIA-1. Granule fusion takes approximately 30 seconds and they remain fused for over 4 minutes. The association shown here, between GFP-TIA-1 and the viral RNA, is not as transient as shown earlier in Fig. 3, given that the green signal follows the fusion process. These images suggest that there are multiple types of interactions, including an association of RNA binding protein with the RNA granules. Scale bar, 1 μ m.



Supplementary Figure 9: Time-lapse imaging of granule splitting. Time-lapse imaging reveals, over a 3 minute period, the splitting of a viral RNA granule that is well associated with GFP-TIA-1. Over the 3 minute period, the splitting occurs rapidly, under 15 seconds; once split, the granules remained separated during our imaging period. Again, the association shown here, between GFP-TIA-1 and the viral RNA, is not as transient as shown earlier in Fig. 3, given that the green signal follows the splitting process. Scale bar, 1 μm .



Supplementary Figure 10: Live-dead assay assessment of the effects of SLO on A549 cells. Results from the application of a two-color fluorescence live-cell viability assay (Invitrogen) to A549 cells not exposed to SLO and those that were exposed to 0.2 U/ml for 10 minutes. From images it can be seen that SLO exposure does not change cell morphology and is associated with minimal cell death. From statistics generated from over 700 cells in each group, 98.85 percent of the cells that were *not* exposed to SLO were alive, while 96.85 percent were alive after SLO exposure. SLO was associated with only a two percent increase in cell death over the normally growing cells. (Green cells are living, while red cells are dead.)

RNA target	Ligand	Accession Number & Location within gene
hRSV genomic RNA	5'-biotin- UXTXTT <u>AAAAAXGGGGCAAAXAA</u> -3'	M74568; 39-55;590-606;2323-2339
Human β -actin mRNA		NM_001101.2
Probe 1	5'-biotin- UXTTTX <u>AXAGCACAGCCXGGAXA</u> -3'	494-478
Probe 2	5'-biotin- TTTTTT <u>AUUXCCCGCXCGGCCGXG</u> -3'	696-679
Chicken β -actin mRNA		NM_205518 XM_429312
Probe 1	5'-biotin-TTTTTT <u>GGAGXAACGCGGXGAGXCAGXCAG</u> -3'	57-38 (61-38 Tyagi, 2004)
Probe 2	5'-biotin-TTXTTT <u>CAAXAUCAXCAUCCAXGGC</u> -3'	84-66 (83-66 Tyagi, 2004)
Probe 3	5'-biotin-TTTTTT <u>AGGAXACCXCUUXUGCUCXGG</u> -3'	262-242 (262-240 Tyagi, 2004)
Chicken arp2 mRNA		NM_205224
Probe 1	5'-biotin-TTTTTT <u>UCCXCCCAGCGXGUCCA</u> -3'	130-112
Probe 2	5'-biotin-TTTTTT <u>ACCAAGCXTCCAGCACAC</u> -3'	1280-1261
Probe 3	5'-biotin-TTXXTT <u>CAGXUGAXCUTAXAAUAGG</u> -3'	243-225
Scrambled probe	5'-biotin-TTTTTTTT <u>CUAAXACXGUAXCAUCXGC</u> -3'	
	Boldface: 2'-O-Methyl RNA; X: dT-C6-NH ₂ ; all others are DNA; underline: binding region	

Supplementary Table 1: Ligands for MTRIPs used to target RNA and as a control probe in living cells.

Supplementary Results

Imaging of MTRIPs on glass surfaces: Probes at 2 nM concentrations were immobilized on a glass surface by adding them in growth media to a coverslip well and incubating them for 10 minutes at 37 °C. The mixture was removed, growth medium was added, and the glass surface was imaged. Individual batches of each probe (see Supplementary Fig. 1a), in addition to a mixture of Cy3B and ATTO 647N labeled probes (see inset image Supplementary Fig. 1a), were imaged on the glass surface. Individual probes were identified, and the mean intensity within the diffraction limited spots was plotted as a histogram (Supplementary Fig. 1b). From the images of the probe mixtures, the histograms of each probe, and three-dimensional plots of the intensity of individual probes (Supplementary Fig. 1c), it is clear that the images represented detect single probes and not aggregates.

Single sequence targeting of β -actin mRNA and 3D colocalization with ZBP1: Further evidence that these probes can be used to image native RNA was provided by targeting human β -actin mRNA in motile A549 cells. In this case, when targeting β -actin mRNA only one site, previously identified¹, was used (see Supplementary Table 1). β -actin mRNA, in motile cells, has been described to colocalize with the RNA binding protein, ZBP1² and with F-actin³. Delivering MTRIPs at 30 nM and 1 nM concentrations, we easily observed those associations in cells fixed post live-cell hybridization and stained with an anti-ZBP1 antibody. In Supplementary Fig. 2 a,b outstretched pseudopods showed colocalization in both the image and in the intensity profile plot, while in Supplementary Fig. 2 c,d, MTRIPs were observed aligned with stained stress fibers (see merge as well as inset image). From the widefield deconvolved 2D images, 3D images were reconstructed in Improvion's Volocity software (Supplementary Fig. 3a). From the overlap of voxels generated in Volocity, the Manders overlap coefficient was

calculated as 0.92, (Supplementary Fig. 3b) clearly indicating colocalization in three dimensions between human β -actin mRNA detected with MTRIPs and ZBP1.

Imaging of arp2 and β -actin mRNA and ZBP1 in primary chicken embryonic fibroblasts (CEF): In order to show the flexibility and applicability of this method, simultaneous imaging of two mRNAs in primary chicken embryonic fibroblasts (CEF) was performed (Supplementary Fig. 4). CEFs were used because they have been a well-studied model system for studying RNA localization³. Three MTRIPs targeting separate sequences on β -actin mRNA and arp2 mRNA were chosen based on both previous sequences used⁴ and mFOLD folding of arp2 mRNA, where large single stranded loop sections were chosen. Even though only 2 probes per RNA are necessary for specific detection in non-clustered RNA (see Fig. 2), in order to optimize the signal for future dynamics studies, three probes per RNA were utilized (Supplementary Table). β -actin targeted MTRIPs were labeled with ATTO 647N and arp2 targeted probes with Cy3B. Probes were delivered into CEFs (30 nM for each probe) for 10 minutes via SLO permeabilization; twenty minutes after delivery one set of cells was fixed for ZBP1 immunostaining while the other set utilized for live-cell imaging. In Supplementary Fig. 4a an extended view image of arp2 (red) and β -actin (blue) mRNA, and ZBP1 (green) in a motile primary CEF is presented. Intensity profiles (Supplementary Fig. 4a,b) through two cross-sections of the extended view demonstrate two types of localization; in the perinuclear region, β -actin mRNA signal is not correlated with the arp2 mRNA signal, especially from approximately pixel 100 to 225 in profile 1 and from 100 to 150 and 175 to 225 in profile 2; ZBP1 and β -actin mRNA are correlated within these same regions. While, from a single plane image (Supplementary Fig. 4 c-f) of the cell near the glass surface, (Supplementary Fig. 4 c,d); colocalization of arp2 (red) and β -actin (blue) mRNA, and ZBP1 (green) can be observed within the lamellipodium, especially at the leading edge. Similar colocalization of the RNAs was observed in the live-cell image within a cellular protrusion and along the cellular periphery; this was demonstrated quantitatively in the intensity profiles (Supplementary Fig. 4 g,h). In addition, in order to demonstrate that SLO delivery does not significantly affect even primary cells, phase-contrast images of representative cells before and after SLO exposure (Supplementary Fig. 4i), show no changes in cell morphology or their ability to create lamellipodia, necessary for motility.

The localization of both mRNA within the lamellipodia shown here, is consistent with a previous report on their localization⁵; our data though suggests that the two mRNA are likely separate within the perinuclear region but are packaged together when transported to protrusions or lamellipodia. This is reasonable given a report that arp3 mRNA likely contain a ZBP1 binding site⁶, and from our own sequence alignments (data not shown), arp2 mRNA are also likely to contain one. From the one previous report⁵, they claim these mRNA localize but do not colocalize, but from our examination of their data (data not shown), they may have underestimated the amount of colocalization.

Targeting of hRSV genomic RNA and 3D colocalization with N protein: In order to show these probes can target viral RNA molecules specifically within living cells, MTRIPs targeted to the genomic RNA of hRSV and β -actin mRNA were assembled, delivered via SLO into infected and non-infected cells, fixed in paraformaldehyde post-hybridization and stained for known RNA binding proteins or colocalized molecules. This experiment was performed in order to confirm the probes were binding to functional, biologically relevant populations of RNA. Intensity profiles, as well as merged images from a single image plane, are displayed to show RNA-protein colocalization. A single probe was used to target the gene-end-intergenic-gene-start sequence of the hRSV genome, which has 3 exact repeats⁷ (see Supplementary Table 1). When delivered at 30 nM concentrations, localized signal was observed within 10 minutes. Following fixation and staining, the RNA signal was observed to be colocalized (yellow) with the

nucleocapsid (N) protein, in the infected A549 cells. This colocalization was observed in the merged image as well as in an intensity profile intersecting granules (Supplementary Fig. 5 a,b), while in the non-infected cells, only background signal was evident (Supplementary Fig. 5 c,d). The hRSV N protein was chosen because it is known to associate strongly with hRSV viral genomic RNA. This experiment was repeated and followed by 3D imaging with a laser scanning confocal microscope; 2D images were reconstructed in 3D in Improvision's Volocity software (Supplementary Fig. 6). From the overlap of voxels generated in Volocity, the Manders overlap coefficient was calculated as 0.65, clearly indicating colocalization in three dimensions between the viral RNA detected with MTRIPs and the nucleocapsid protein.

Comparison of tetravalent MTRIPs with monovalent ligands: Tetravalent MTRIPs and monovalent probes (single multiply-labeled ligand) both targeted to hRSV genomic RNA were delivered via SLO, each at 30 nM, into separate wells of A549 cells, each infected from the exact same vial of virus, 24 hrs post-infection. The cells were then fixed in 4% paraformaldehyde and imaged via laser scanning confocal. From the reconstructed 3D images of the cells (see extended view images of the cells in Supplementary Fig. 7a), the number of viral RNA granules could be counted for each probe type. It should be noted that even though the number of granules detected is statistically similar via the Wilcoxon-Mann-Whitney test, the photomultiplier voltage on the laser scanning confocal microscope was approximately 4 times higher for the monovalent probe, which was expected. By combining 4 ligands, the resulting MTRIPs were 4 times brighter, a necessity for the live-cell imaging in Fig. 3. From the results of counting RNA granules from over 30 cells (Supplementary Fig. 7b) for both the tetravalent and monovalent probes, the statistical similarity of the two populations could be estimated using the Wilcoxon-Mann-Whitney test. From this test, the resulting p value of 0.87 was determined, which conclusively demonstrates that the samples originated from the same population. This conclusively shows that MTRIPs do not significantly aggregate RNA; RNA aggregation would have resulted in the detection of different numbers of RNA granules.

Additional vRNA-TIA-1 Interactions Observed: In addition to the transient behaviour shown in Fig. 3, we also noted that GFP-TIA-1 was visible on some of the viral RNA granules approximately 20 to 30 minutes after sodium arsenite treatment. Their association was confirmed by capturing video images of RNA granules during both a fusion (Supplementary Fig. 8 and Video 4) and splitting event (Supplementary Fig. 9 and Video 5), and observing the protein follow the same dynamic course as the RNA. The overlap is not perfect, suggesting that only some of the RNA in the granule may be in contact with GFP-TIA-1, but the association is quite obvious. This finding suggests that there may be multiple mechanisms by which TIA-1 interacts with RNA, in a transient, granule-granule manner (Fig. 3), which may depend on granule size, and also through a more stable event, driven by RNA-protein binding.

Effect of SLO on A549 cells: A standard live/dead viability/cytotoxicity assay (Invitrogen L-3224) was performed to assess the effect of SLO on A549 cells (see Supplementary Fig. 10). The assay was performed on normally growing cells and cells exposed to 0.2 U/ml of activated SLO for 10 minutes. From the results in Supplementary Fig. 10, it can be seen that SLO exposure does not change cell morphology and is associated with minimal cell death (green cells are living while red cells are dead). From statistics generated from over 700 cells in each group, 98.85 percent of the cells that were not exposed to SLO were alive, while 96.85 percent were alive after SLO exposure. SLO was associated with only a two percent increase in cell death over the normally growing cells. This is consistent with a previous live/dead assay performed on Hela cells reported by Paillason et al. (1997). They reported 95% alive in normally growing cells, and 93% alive when exposed to SLO⁸.

Quantification of a specific native mRNA within a live cell: In order to use this technique to accurately quantify the number of a specific native mRNA within a cell in a wider variety of granules, additional information will need to be obtained, that are beyond the scope of this paper. Currently using MTRIPS we can easily distinguish between single probes (377 ± 27 a.u.) and single RNAs (two probes, 677 ± 55 a.u.) and demonstrated that statistically. Once an mRNA is packaged into larger granules it would be difficult, at this point, to know if the fluorescence signal remains linear with RNA number. Non-linearity in the signal within a granule as a function of mRNA number could likely be caused by many effects, such as collisional quenching, and may require calibration-based compensation or post-processing depending on the contents and size of the granule and its location within the cell⁹. Future experiments using time-resolved fluorescence microscopy could be performed to evaluate the effects of quenching and correlate them with granule size and location within the cell.

1. Abe, H. & Kool, E.T. Flow cytometric detection of specific RNAs in native human cells with quenched autoligating FRET probes. *Proc Natl Acad Sci U S A* **103**, 263-268 (2006).
2. Farina, K.L., Huttelmaier, S., Musunuru, K., Darnell, R. & Singer, R.H. Two ZBP1 KH domains facilitate beta-actin mRNA localization, granule formation, and cytoskeletal attachment. *J Cell Biol* **160**, 77-87 (2003).
3. Oleynikov, Y. & Singer, R.H. Real-time visualization of ZBP1 association with beta-actin mRNA during transcription and localization. *Curr Biol* **13**, 199-207 (2003).
4. Tyagi, S. & Alsmadi, O. Imaging native beta-actin mRNA in motile fibroblasts. *Biophys J* **87**, 4153-4162 (2004).
5. Mingle, L.A. et al. Localization of all seven messenger RNAs for the actin-polymerization nucleator Arp2/3 complex in the protrusions of fibroblasts. *J Cell Sci* **118**, 2425-2433 (2005).
6. Shestakova, E.A., Singer, R.H. & Condeelis, J. The physiological significance of beta - actin mRNA localization in determining cell polarity and directional motility. *Proc Natl Acad Sci U S A* **98**, 7045-7050 (2001).
7. Player, M.R., Barnard, D.L. & Torrence, P.F. Potent inhibition of respiratory syncytial virus replication using a 2-5A-antisense chimera targeted to signals within the virus genomic RNA. *Proc Natl Acad Sci U S A* **95**, 8874-8879 (1998).
8. Paillason, S. et al. In situ hybridization in living cells: detection of RNA molecules. *Exp Cell Res* **231**, 226-233 (1997).
9. Lakowicz, J.R. Principles of Fluorescence Spectroscopy, Edn. 3. (Springer Science+Business Media LLC, New York, NY; 2006).